of the fundamental processes that occur during laser irradiation which promote changes in the physical and chemical structure of dental enamel. For safe and efficient use of any laser in the dental clinic, the absorption and redistribution of energy during laser irradiation of dental enamel must be well characterized which requires accurate knowledge of the relevant optical properties of dental enamel. Since dental enamel strongly absorbs infrared light, scattering can be neglected, and the relevant optical properties are the reflectance and absorption coefficient. Due to the strong absorption and the brittleness of dental enamel, sufficiently thin enamel sections cannot be prepared to allow conventional transmission experiments that determine absorption coefficients in the infrared region from 9–10 μm. By modeling the time resolved thermal emission of dental enamel irradiated with a pulsed CO_2 laser, we have estimated the absorption coefficient at 9.6 μm to be approximately 8000 cm^{-1}. To verify the model, dental enamel was irradiated with 10.3 and 10.6 μm light where the absorption coefficients can be determined by direct transmission experiments. In addition to the absorption coefficient, the mathematical model incorporates the spatial and temporal profile of the laser pulse and the spectral response and variable emissivity in the detection region.

After confirming the capability of the model to predict the temperature rise and thermal emission of laser irradiated dental enamel, the model was used to correlate the depth of modified enamel with the temperature rise at that depth. The mineral phase of enamel is a highly substituted hydroxyapatite with the principal substitution of carbonate for either the phosphate or the hydroxyl group. These substitutions result in a greater solubility in acid. Carbonate loss of irradiated enamel was measured as a function of depth by polishing the enamel at 1 μm intervals and subsequently employing infrared spectroscopy to ascertain the strength of the carbonate band. In other experiments, carbonate loss has been correlated to a reduction in the progression of *in vitro* caries-like lesion formation by a chemical model that approximates the demineralization and remineralization cycle that occurs in the oral cavity. The depth of carbonate loss is dependent upon the absorption coefficient of enamel, the laser pulse duration, and the energy deposited. The temperature rise needed to eliminate carbonate from the hydroxyapatite structure is approximately 400°C. This study provides fundamental information that can be used to determine appropriate laser parameters for safe and efficient use in clinical dentistry.

This work was supported by NIH/NIDR Grants DE09958 and DE12091.

*Laboratory for Laser Energetics, University of Rochester, Rochester, New York 14623-1299 USA; E-mail: seka@lle.rochester.edu

Ultrafast Optics, Optoelectronics, and Applications

CWF10

Metal-semiconductor-metal traveling-wave-photodetectors

Jin-Wei Shi, Chi-Kuang Sun, Ying-Jay Yang,* *Graduate Institute of Electro-Optical Engineering, National Taiwan University, Taipei 10617, Taiwan, ROC; E-mail: sun@cc.ee.ntu.edu.tw*

The bandwidth/efficiency of traditional vertically-illuminated metal-semiconductor-metal (MSM) photodetectors are limited by RC time constant, carrier drift time, and carrier recombination time. In order to shorten the carrier transit/recombination time, 25 nm finger spacing has been fabricated by using high resolution e-beam lithography on Low-Temperature (LT) GaAs.[1] Although this device has large bandwidth, it suffers relatively low quantum efficiency due to the high metal-reflection loss. Besides, the fabrication processes are expensive and complex. Recently, transparent metal ITO (indium-tin-oxide) was used to overcome the high-metal-reflection loss.[2] However, the quantum efficiency is still low due to the fact that only the photoexcited carriers near semiconductor surfaces can be collected. Another major problem for most vertically illuminated MSM photodetectors is RC bandwidth limitation. An alternative approach to overcome RC bandwidth limitation is traveling-wave-limitation. An alternative approach to overcome RC bandwidth limitation is traveling-wave-photodetector (TWPD).[3] In TWPD, the RC bandwidth limitation is replaced by velocity mismatch between optical wave velocity (V_o) and electrical wave velocity (V_e). A bandwidth of 560 GHz and a quantum efficiency of 8% has been reported using LT-GaAs TWPDs.[4] In this paper we propose and analyze a new device, the MSM traveling-wave-photodetector (MSM-TWPD). Instead of traveling at a slow-wave mode, the electrical wave will propagate as ordinary waves in our new device structure. The velocity-mismatch-limited bandwidth B_{vm} can thus be greatly enhanced (usually on the order of 7 THz) compared with that of p-i-n TWPDs (usually on the order of 2 THz). With an appropriate device design, the side-pumped carriers will not only be completely absorbed but be generated close to the device surface, thus greatly

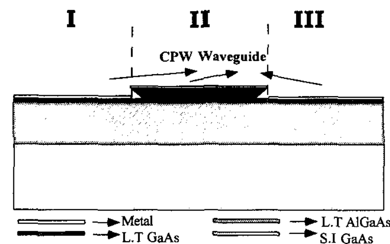

CWF10 Fig. 1. Cross sectional diagram of MSM-TWPD. This structure can be easily fabricated by wet etching and self-aligned metal evaporation.

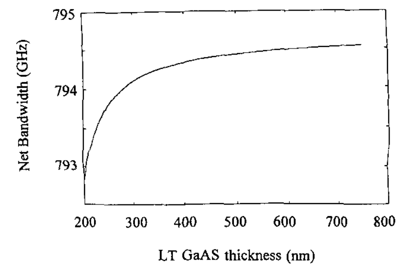

CWF10 Fig. 2. Net bandwidth v.s. LT GaAs layer thickness. The bandwidth is dominated by carrier lifetime, and varies lightly with different layer thickness.

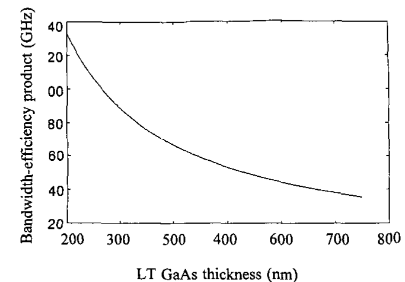

CWF10 Fig. 3. Bandwidth-efficiency product v.s. LT GaAs layer thickness. The efficiency decreases when the layer thickness increases. The coupling loss is neglected.

increasing the quantum efficiency compared with vertically illuminated MSM photodetectors.

The cross sectional schematic of this device is shown in Fig. 1. It is made by a thin LT GaAs layer which is grown on a LT semi-insulating AlGaAs layer[5] (for wave guiding). This structure can be fabricated easily by under-cut wet etching, and directly evaporating indium on LT GaAs as contact metal.[6] Complex fabrication processes can thus be easily avoided. In a TWPD, the velocity-mismatch-limited bandwidth will usually increase with higher V_e.[3] In p-i-n TWPD, the electrical waves propagate in slow wave modes due to heavily doped p^+/n^+ regions.[7] On the other hand, in MSM-TWPD, the electrical wave on coplanar waveguides (CPW) will propagates an ordinary quasi-TEM mode, due to semi-insulating substrate materials (including LT GaAs LT AlGaAs). This implies that B_{vm} of MSM TWPD should be much higher than that of p-i-n TWPD. Another bandwidth limitation is carrier lifetime. Assuming that recombination current is exponentially decayed, we can define the lifetime limited bandwidth B_{mL} as $B_{mL} = \frac{1}{2\pi\tau}$ where τ is the carrier lifetime of LT GaAs. Figure 2 shows the calculated net bandwidth, considering both B_{mL} and B_{vm}, as a function of LT GaAs layer thickness with a LT GaAs carrier lifetime of 200 fs. We let the thickness of regions I and III in figure 1 to vary between 200 nm and 750 nm and the thickness of region II to be 1.5 times that of I and III. In such case most optical power concentrates near electrodes, and higher quantum efficiency can be excepted. With a B_{vm} of 7 THz, the net band-

width is found to be completely dominated by B_{mL} to be on the order of 790 GHz in our proposed structure. Figure 3 shows the calculated bandwidth-efficiency product as a function of LT GaAs layer thickness, neglecting coupling loss. With a side-illumination structure, metal reflection loss can be neglected and complete absorption can be achieved. The quantum efficiency should thus be limited only by the ratio between carrier lifetime and carrier drift time. We estimate the drift distance by averaging different carrier travelling distances between two electrodes. With a carrier saturation velocity of 90 nm/ps, a quantum efficiency of 0.17 and a bandwidth-efficiency product of 132 GHz can be achieved with a LT GaAs layer thickness of 200 nm.

This work is supported by National Science Council (NSC 88-2218-E-002-038).

*Department of Electrical Engineering, National Taiwan University, Taipei 10617, Taiwan, ROC

1. S.Y. Chou, Mark Y. Liu, IEEE Journal of Quantum Electronics **28,** 2358 (1992).
2. S.J. Wook, *et al.*, IEEE Photonics Technology Letters **5,** 1313 (1993).
3. K.S. Giboney, *et al.*, IEEE Journal of Selected Topics In Quantum Electronics **2,** 622 (1996).
4. Y.J. Chiu, *et al.*, IEEE Photonics Technology Letters **10,** 1012 (1998).
5. W. Feng, *et al.*, Proceedings of SPIE **2896,** 173 (1996).
6. F.W. Smith, *et al.*, Appl. Phys. Lett. **54,** 890 (1989).
7. Y.R. Kwon, *et al.*, IEEE Trans. On Microwave Theory And Tech., *MTT-35,* 545 (1987).

CWF11

Enhancement of optical nonlinearity for short wavelength (~1.5 μm) intersubband transitions by *n*-doped InGaAs/AlAsSb MQW

Tomoyuki Akiyama, Arup Neogi, Haruhiko Yoshida, Osamu Wada, *The Femtosecond Technology Research Association, 5-5 Tokodai, Tsukuba 300-2635, Japan; E-mail: akiyama@festa.or.jp*

For the application of ultrafast optical devices in future OTDM or WDM network, the intersubband transition (ISBT) provides attractive features such as large optical nonlinearity with ultrafast response. The material system available for achieving ISBT at optical communication wavelength is, however, limited. Although the ISBT at 1.5 μm have been reported in $In_{0.53}Ga_{0.47}As/AlAs$[1,2], the large lattice mismatch makes it difficult to grow, and the electron leakage into the X valley of the barriers[2] reduces the absorption. Alternatively, GaN/AlN[3] and InGaAs/AlAsSb[4] have attracted attention because of their large ΔE_c, reduced electron leakage, and the design flexibility of the lattice-matched system. ISBT by use of InGaAs/AlAsSb has been recently observed by our group[5] at 1.5 μm. However, its optical nonlinearity has not yet been reported. We show that the InGaAs/AlAsSb exhibits a larger nonlinearity than GaN due to the large dephasing time (T_2) stemming from the small effective mass (m_e^*) and LO phonon energy ($\hbar\omega_{LO}$), and that the conduction band nonparabolicity plays only a minor role.

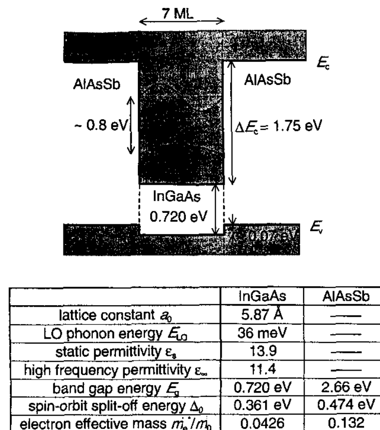

	InGaAs	AlAsSb
lattice constant a_0	5.87 Å	——
LO phonon energy E_{LO}	36 meV	——
static permittivity ε_s	13.9	——
high frequency permittivity ε_∞	11.4	——
band gap energy E_g	0.720 eV	2.66 eV
spin-orbit split-off energy Δ_0	0.361 eV	0.474 eV
electron effective mass m_e^*/m_0	0.0426	0.132

CWF11 Fig. 1. Schematic of band diagram and material parameters of $In_{0.53}Ga_{0.47}/As/AlAs_{0.56}Sb_{0.44}$ quantum well.

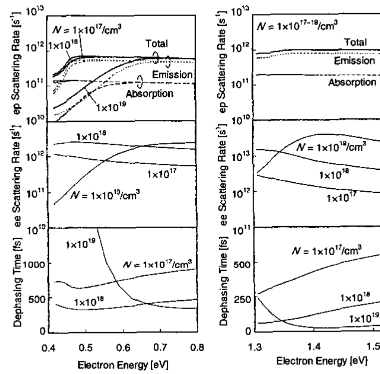

CWF11 Fig. 2. Calculated electron-LO phonon (ep) scattering rate τ_{ep}^{-1}, electron-electron (ee) scattering rate τ_{ee}^{-1}, and dephasing time T_2 of the (a) first and (b) second subbands for three different electron densities *N*.

In calculating T_2, both the electron-LO phonon (τ_{ep}) and electron-electron (τ_{ee}) scatterings were considered. τ_{ep} was calculated based on the dielectric continuum model. Fermi golden rule was used with the screened Coulomb potential[6] to calculate τ_{ee}. Saturation intensity (I_s) was evaluated using perturbational density matrix theory.

The schematic band diagram and the material parameters are shown in Fig. 1. Figure 2 shows the calculated τ_{ee}^{-1}, τ_{ep}^{-1}, and T_2 for the (a) first and (b) second subbands. At higher electron density $N (\sim 1 \times 10^{19}\ cm^{-3})$, filling of the final states and the Coulomb screening dominate the scattering rate, resulting in decrease in τ_{ee}^{-1}. Similar reduction was observed for τ_{ep}^{-1} at increased doping level and is explained by the state filling. These combined effects produce an extremely large T_2 exceeding 1 ps at $N = 1 \times 10^{19}\ cm^{-3}$. This T_2 is much larger than that for GaN/AlN (80 fs)[3], and is a result of the smaller m_e^* *and* $\hbar\omega_{LO}$ *for the InGaAs/AlAsSb MQW.*

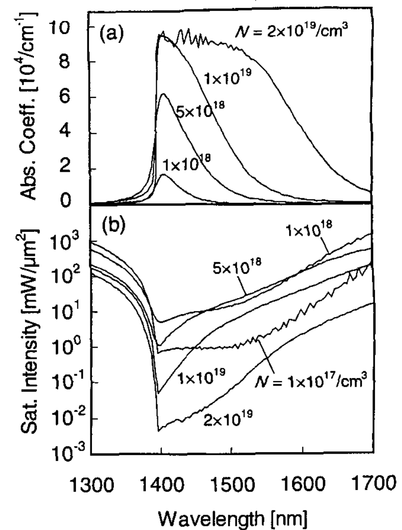

CWF11 Fig. 3. (a) Linear absorption coefficient α_0 and (b) saturation intensity I_s, for different electron densities *N*.

Figure 3(a) shows that the linear absorption coefficient α_0 increases with *N* until it saturates to $0.95 \times 10^5\ cm^{-1}$ and broadens due to the nonparabolicity. On the other hand, such saturation and broadening are not significant for GaN/AlN. In spite of the saturated absorption for InGaAs/AlAsSb, the absorption is enhanced by one order of magnitude in comparison with commonly accepted values for the interband transitions (IBTs). This is supported by our recent experimental observation of α_0 ($\sim 4 \times 10^3\ cm^{-1}$) comparable to that for IBTs in a sample nominally *n*-doped by $3 \times 10^{18}\ cm^{-3}$, still leaving room for improvement[7].

In Fig. 3(b), an I_s as low as 0.04 mW/μm^2 is achieved by increasing *N* up to $1 \times 10^{19}\ cm^{-3}$. When compared to GaN/AlN, this is at least two orders of magnitude larger. Since I_s is approximately proportional to T_2^{-3}, such a low I_s is explained by larger T_2 as indicated in Fig. 2, which compensates the increase of I_s due to the larger nonparabolicity. It is interesting to note that I_s for IBTs is typically 0.1 mW/μm^2 with a response of ~1 ns. In contrast, the estimated intersubband relaxation time is as short as 1.5 ps.

1. Y. Hirayama, J.H. Smet, L.-H. Peng, C.G. Fonstad, and E.P. Ippen: Appl. Phys. Lett. **63,** 1663, (1993).
2. T. Asano, S. Noda, T. Abe, and A. Sasaki: J. Appl. Phys. **82,** 3385 (1997).
3. N. Suzuki, and N. Iizuka: Jpn. J. Appl. Phys. **36,** L1006 (1997).
4. H. Asai, and Y. Kawamura: Proc. Int. Conf. InP and Related Materials, 493 (1992).
5. T. Mozume, H. Yoshida, A. Neogi, and M. Kudo: Post Deadline Papers of Int. Conf. InP and Related Materials, 9 (1998).
6. S.M. Goodnick, and P. Lugli: Appl. Phys. Lett. **51,** 584 (1987).
7. T. Mozume, H. Yoshida, A. Neogi, and M. Kudo: Jpn. J. Appl. Phys. **38,** 2 (1999).